

Breaking Free from Fusion Rule: A Fully Semantic-driven Infrared and Visible Image Fusion

Yuhui Wu, Zhu Liu, Jinyuan Liu, Xin Fan, *Senior Member, IEEE*, Risheng Liu, *Member, IEEE*

Abstract—Infrared and visible image fusion plays a vital role in the field of computer vision. Previous approaches make efforts to design various fusion rules in the loss functions. However, these experimental designed fusion rules make the methods more and more complex. Besides, most of them only focus on boosting the visual effects, thus showing unsatisfactory performance for the follow-up high-level vision tasks. To address these challenges, in this letter, we develop a semantic-level fusion network to sufficiently utilize the semantic guidance, emancipating the experimental designed fusion rules. In addition, to achieve a better semantic understanding of the feature fusion process, a fusion block based on the transformer is presented in a multi-scale manner. Moreover, we devise a regularization loss function, together with a training strategy, to fully use semantic guidance from the high-level vision tasks. Compared with state-of-the-art methods, our method does not depend on the hand-crafted fusion loss function. Still, it achieves superior performance on visual quality along with the follow-up high-level vision tasks.

Index Terms—Image fusion, semantic-level fusion network, semantic-driven training strategy.

I. INTRODUCTION

INFRARED and visible image fusion (IVIF), referring to providing the typical characteristics from source images, has been witnessed rapid development in recent years. IVIF can effectively break the limitation of information loss from single sensor and plays an important role for the follow-up high-level vision tasks, e.g., object detection [1], semantic segmentation [2] and so on. Unfortunately, there are few works [3]–[5] to bridge high-level semantic tasks with image fusion. In this paper, rather than explicitly construct fusion rules for IVIF, we propose a generic semantic-driven learning paradigm to investigating task-specific image fusion.

In the past, traditional fusion methods prevailed, including [6]–[13]. Recently, deep learning-based methods have shown great potential in numerous image-processing fields [14]–[16] by their powerful nonlinear feature extraction capabilities.

This work is partially supported by the National Key R&D Program of China (2020YFB1313503), the National Natural Science Foundation of China (Nos. 61922019 and U22B2052), the Fundamental Research Funds for the Central Universities and the Major Key Project of PCL (PCL2021A12). (*Corresponding author: Risheng Liu.*)

Yuhui Wu and Zhu Liu are with the School of Software Technology, Dalian University of Technology, Dalian 116024, China. (wuyuhui63@hotmail.com; liuzhu_dlut@mail.dlut.edu.cn).

Jinyuan Liu is with the School of Mechanical of Engineering, Dalian University of Technology, Dalian 116024, China. (e-mail: atlantis918@hotmail.com).

Xin Fan and Risheng Liu are with the DUT-RU International School of Information Science & Engineering, Dalian University of Technology, Dalian 116024, China. They are also with Peng Cheng Laboratory, Shenzhen 518052, China. (e-mail: xin.fan@dlut.edu.cn; rslu@dlut.edu.cn).

Learning-based IVIF approaches achieve promising performance based on the design of various fusion rules and loss functions. We can roughly divide current learning schemes into two categories: fusion-rule based methods [17]–[20] and end-to-end learning schemes [3], [21]–[30].

In specific, the first kind of fusion methods rely on the manually designed rules to aggregate the modal feature approximately. These methods firstly utilize the auto encoder mechanisms to extract and reconstruct multimodal features to sufficiently learn the significant feature extraction. Then they develop various fusion rules for feature fusion, e.g., weighted average, summation, maximum selection, and ℓ_1 norm. For instance, Li *et al.* [17] pioneered the dense blocks as the learnable auto-encoder and utilized the weighted-average strategy to fuse modal features. After that, Li *et al.* [18] also provide spatial/channel attention mechanisms as the fusion strategies to fuse features with nested connections. Subsequently, Liu *et al.* [31] introduces the edge attention guided auto-encoder to extract feature and adopts the simple fusion rules.

We can obviously observe that, current methods rely on the appropriate fusion strategies to guide the feature fusion. However, these fusion strategies are not sensitive to the diverse data distribution and are easy to induce visual artifacts and blurs. More importantly, the manual design of fusion strategies are too fragile to preserve suitable modal characteristics for supporting follow-up high-level vision tasks.

Instead of manually designed fusion rules, end-to-end learning methods are proposed to establish the connection between source and fused images directly. Specifically, architectures and loss functions are two challenging stumbling stones for these methods. Existing methods concentrate on designing architectures based on the current effective practices, rather than considering the particular properties of fusion tasks. For example, dense blocks [21] and residual blocks [4] are widely utilized for IVIF. Besides, diverse loss functions are proposed to enforce different principles for IVIF. Typically, Ma *et al.* [24] introduce the dual generative adversarial criterion to push the generated images as similar as the source images. Xu *et al.* [21] propose the feature-level measurement to endow the richness of information into fused images. Tang *et al.* [4] uses the max-choosing rule to design loss function, but is limited in extreme scenes (e.g., glare and fog).

Though visually appealing results which can acquire remarkable statistical metrics are obtained. These loss functions coupled with training strategies make the methods more complex. Furthermore, these architectures cannot effectively extract the modal characteristics, limited by the local awareness of convolution networks. We argue that both two categories of

methods are designed to improve the visual quality of fusion, neglecting the requirement of follow-up semantic tasks.

To partially mitigate these issues, in this letter, we propose a semantic-driven fusion method. Instead of considering the image fusion as an independent task, we fully leverage the guidance of high-level semantic tasks to reserve the beneficial information and reduce the conflicts. In this way, our fused results not only highlight the comprehensive information, but also facilitate the following semantic tasks. To be concrete, we first propose a multi-scale fusion network with self-attention mechanism to sufficiently aggregate the modal features. Multi-scale extraction can effectively combine features in a coarse-to-fine manner from the scene structure to context details. Self-attention mechanism is to establish the long-range dependency of multi-modal features, better depict the global representation of salient targets. Then we introduce a correlated regularization to describe the relationships between source images and fused images. Based on this, we only utilize the criterion of high-level vision tasks to train both the fusion and high-level networks. Thus, this strategy emancipates the experimental design of fusion rules, discards the restriction of modal statistic metrics and drastically improves the performance of high-level vision tasks. We summarize the core contribution as follows:

- A multi-scale self-attention-based image fusion network is proposed to effectively represent the global structures in a coarse-to-fine manner.
- Imposing a correlated regularization, a fully semantic-driven training strategy is introduced to break free from handcrafted fusion rules.

II. THE PROPOSED METHOD

A. Network Architecture

While some previous works focus on pursuing high efficiency at the expense of the fitting ability of the fusion network, it does not work well to utilize the semantic guidance from the follow-up high-level vision tasks. In contrast, we hypothesize that the fusion network should be capable of semantic understanding to achieve flexible fusion effects among various semantic classes.

To this end, we employ the multi-scale mechanism from [18] to deal with the textural details and semantic information, respectively. As shown in Fig. 1, we use the downsampling (i.e. max-pooling) operations to obtain feature maps of different resolutions. Among them, the shallow layer feature maps contain more textures information, while the deep layer feature maps contain more semantic information.

On the other hand, to fuse the extracted cross-modal feature maps, we devise a generic fusion block based on the efficient self-attention [32]. As shown in the bottom of Fig. 1, the fusion block consists of two self-attention modules, which can capture and reinforce the useful components in the global receptive field. In the self-attention module, we reshape the feature maps of $\mathbb{R}^{H \times W \times C}$ to vectors of $\mathbb{R}^{N \times C}$, where $N = H \times W$. Then, we use the linear layers to encode the vectors into query Q, key K, and value V. We get the attention map by a matrix multiplication $K^T V$, then we acquire the final attention result $Q \text{Softmax}(K^T V)$. The strengthened component is obtained

by element-wise multiplying the attention result and the input feature maps. To reserve the detail information, we further introduce a residual connection.

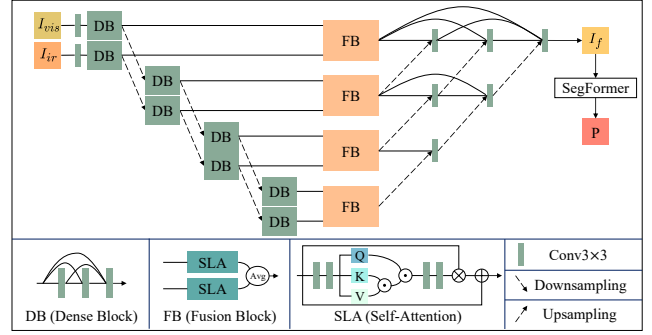


Fig. 1. The workflow of the proposed method. Avg , \otimes and \oplus represent the computation of element-wise average computation, multiplication, and addition, respectively. \odot means matrix multiplication. P denotes the prediction.

B. Training Strategy

Existing end-to-end deep-learning methods focus on devising fusion rules to acquire visually appealing results. Unfortunately, hand-crafted fusion rules are heavily limited to the scene and cannot meet the essential requirement of follow-up semantic tasks. To address this issue, we develop a semantic-driven training strategy to emancipate the manual design.

1) *Warm-start phase*: Jointly training both the fusion and segmentation networks is an intuitive strategy. However, at the beginning of training, the parameters of the fusion model are randomly initialized and thus cannot provide meaningful fused images for the segmentation network to handle. Consequently, the training process deviates from our expectations.

To address this issue, we use an average strategy to pre-train the fusion model to obtain a malleable initialization. This learning procedures can be formulated as

$$\min_{\theta} \mathcal{L}_{WS}(\mathcal{N}_F(I_{vis}, I_{ir}; \theta)), \quad (1)$$

where \mathcal{N}_F is the fusion network with learnable parameters θ , I_{ir} and I_{vis} denote infrared image and visible image, respectively. After this phase, we obtain θ' , which can fuse the source images into substantially average and meaningful results for the next training procedure.

2) *Semantic training phase*: In this phase, we fine-tune the fusion network by jointly training with the segmentation network, which can be formulated as

$$\min_{\theta, \omega} \mathcal{L}_{ST}(\mathcal{N}_S(\mathcal{N}_F(I_{vis}, I_{ir}; \theta'); \omega)), \quad (2)$$

where the \mathcal{N}_S is the semantic segmentation network with learnable parameters ω . The semantic segmentation task will learn to adjust the proportion of infrared and visible components away from the average fusion state.

It is instructive to note that the fusion model without additional constraints is unstable, resulting in degraded segmentation performance. To mitigate this, we design an auxiliary regularization loss function to constrain the fusion model for utilizing far-reaching semantic guidance.

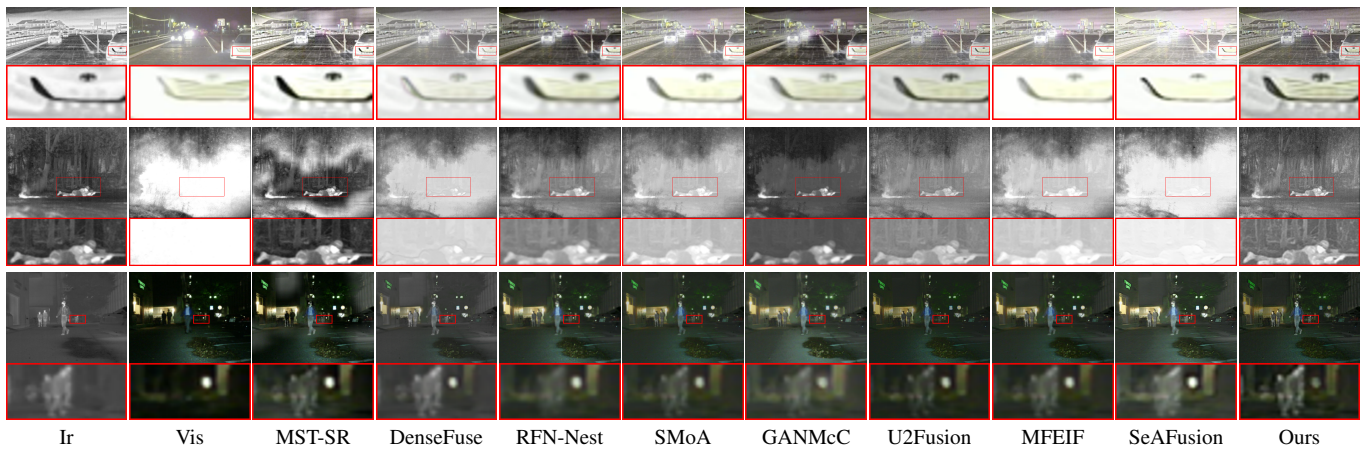


Fig. 2. Qualitative comparison with state-of-the-art fusion methods. The three rows of results are from the RoadScene, TNO, and MFNet datasets, respectively.

TABLE I
PER-CLASS SEGMENTATION RESULTS ON THE MFNET DATASET. THE BEST RESULT IS IN RED WHEREAS THE SECOND BEST ONE IS IN BLUE.

Method	Car		Person		Bike		Curve		Car Stop		Color Cone		Bump		mAcc	mIoU
	Acc	IoU	Acc	IoU	Acc	IoU	Acc	IoU	Acc	IoU	Acc	IoU	Acc	IoU		
MST-SR	86.25	82.36	74.93	65.40	70.38	60.21	55.39	40.21	29.00	26.28	52.53	47.67	49.71	44.53	57.70	51.65
DenseFuse	87.00	81.46	76.16	68.25	66.09	57.90	57.65	44.43	15.20	13.69	36.73	35.36	39.72	36.76	53.10	48.40
RFN-Nest	89.26	83.49	77.05	67.98	67.85	59.68	44.83	35.23	33.75	28.47	54.10	47.47	46.28	42.73	56.94	51.42
SMoA	89.28	83.13	78.30	69.05	66.44	58.81	48.89	38.43	23.96	22.03	49.31	46.64	47.69	44.80	55.92	51.19
GANMcC	89.81	81.46	77.67	67.82	64.16	57.36	41.91	33.59	23.81	20.85	48.93	45.15	48.38	41.72	54.88	49.51
U2Fusion	89.76	83.86	77.77	68.63	71.10	61.62	49.41	36.76	31.51	28.19	48.89	46.00	55.04	47.49	58.08	52.26
MFEIF	88.30	82.73	76.23	68.26	63.61	57.43	51.48	40.06	27.08	21.97	44.85	42.74	45.90	43.60	55.20	50.51
SeAFusion	89.43	82.76	78.42	67.74	66.07	58.28	52.31	38.56	28.58	24.35	46.73	43.58	47.10	45.12	56.43	50.90
Ours	90.14	85.30	82.27	71.65	73.53	63.08	56.24	44.51	35.92	30.96	53.81	50.61	59.98	47.38	61.24	54.61

C. Loss Function

1) Warm-start loss function: The warm-start fusion loss function can be formulated as: $\mathcal{L}_{WS} = \frac{1}{HW} \|I_f - \frac{I_{ir} + I_{vis}}{2}\|_1$, where H and W denote the height and width of the source image, respectively. I_f is the fused image. $\|\cdot\|_1$ represents the calculation of the ℓ_1 norm.

2) Semantic training loss function: During the semantic training phase, we use the semantic training loss function as follows: $\mathcal{L}_{ST} = \mathcal{L}_{sem} + \lambda \mathcal{L}_{reg}$, where the \mathcal{L}_{sem} is a commonly used cross-entropy loss function, while the \mathcal{L}_{reg} is a regularization term. The λ is used to strike a balance between the two terms. We define the regularization loss function as: $\mathcal{L}_{reg} = \frac{1}{Corr(I_{ir}, I_f) + Corr(I_{vis}, I_f)}$, where $Corr(\cdot)$ denotes the calculation of the correlation of two image tensors.

III. EXPERIMENTS

In this section, we first conduct qualitative and quantitative comparisons on three datasets: MFNet [2], TNO [33] and RoadScene [21]. The competitors include MST-SR [34], DenseFuse [17], RFN-Nest [18], SMoA [19], GANMcC [35], U2Fusion [21], MFEIF [31], and SeAFusion [4]. We also conducted ablation studies to validate the proposed architecture and semantic-driven training strategy.

A. Fusion Results

As shown in Fig. 2, we can see that our method can flexibly preserve abundant and useful textural details, successfully

highlighting the important targets in diverse harsh environment. For instance, persons in our method have sharper edges, and thus stand out from the background, which will be helpful for follow-up segmentation. As for quantitative comparisons,

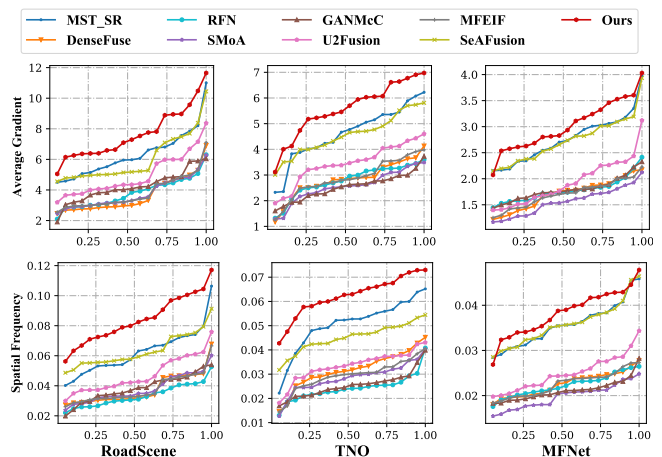


Fig. 3. Statistical evaluation of fusion results. A point (x, y) denotes that there are 100 * x percent of image pairs which have values no more than y.

Our method outperformed others in terms of commonly used statistical evaluation metrics spatial frequency (SF) [36] and average gradient (AG) [37], as shown in Fig. 3. This indicates our results have more information richness, containing more details and high contrast.

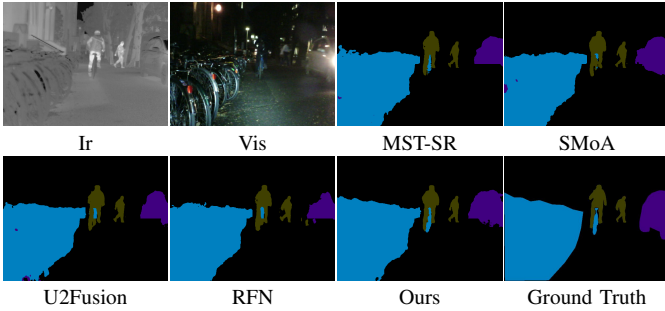


Fig. 4. Qualitative comparison of segmentation results.

B. Segmentation results

We also evaluate the fusion quality from the perspective of semantic segmentation. We trained the same segmentation network (SegFormer-b0) from scratch based on the fused images generated by all comparative methods. As shown in Fig. 4, segmentation model with our method can provide more accurate results, e.g., bikes. In contrast, other methods cannot estimate the shapes of car, interfered by the strong glare. As



Fig. 5. Visual effects using different network architectures.

shown in Table I, our method got the top scores on mAcc and mIoU, indicating our method can intelligently reserve useful information for different semantic classes. Due to the information distortion of other methods, these methods cannot obtain the same accuracy of almost classes.

C. Ablation studies

1) *Analyzing the fusion module:* We conducted experiments including removing the self-attention module (w/o SLA), replacing it with channel attention (CHA) [38], and spatial attention (SPA) [39]. As shown in Fig. 5, persons of our fused result are more natural and conspicuous, which is also demonstrated by segmentation results, as reported in Table II.

TABLE II

SEGMENTATION RESULTS OF DIFFERENT STRUCTURES AND STRATEGIES.

		Car	Person	Car Stop	Bump	mIoU
Structure	w/o SLA	85.11	71.25	21.55	48.96	53.21
	CHA	84.37	71.53	23.86	49.10	53.48
	SPA	84.90	71.30	24.31	48.11	53.78
Strategy	Max-ST	85.66	71.90	23.71	47.91	53.70
	w/o WS	84.43	70.91	13.24	47.19	51.02
	w/o \mathcal{L}_{reg}	85.05	71.28	25.86	46.39	53.40
Ours (Ave-ST)		85.30	71.65	30.96	50.61	54.61

2) *Analyzing the warm-start and regularization loss:* We also provide another warm start, i.e., $\mathcal{L}_{WS} = \frac{1}{HW} \|I_f - \max(I_{ir}, I_{vis})\|_1$, where $\max(\cdot)$ is denoted as element-wise maximum selection. The fused results after the warm-start and semantic training are denoted as “Max”

and “Max-ST”, respectively. The corresponding results of proposed scheme are denoted as “Ave” and “Ave-ST”. As shown in Fig. 6, (b) fails to suppress glare and (c) fails to emphasize pedestrians. After the semantic training phase, they overcome these problems (i.e., (d) and (e)). As shown in Table II, maximum selection fusion rule provides better initialization to preserve the pedestrians and cars. But it fails to deal with other classes, such as car stop. This shows that average fusion rule can provide a more malleable initialization. In addition, we conducted experiments including removing the warm-start phase (w/o WS), and removing the regularization term (w/o \mathcal{L}_{reg}). As shown in Table II, segmentation results are decreased without these strategies.

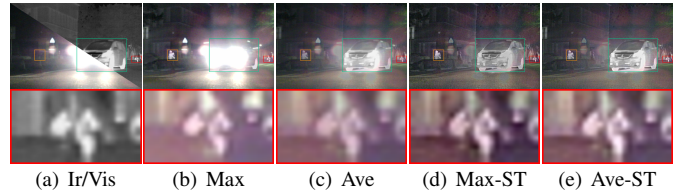


Fig. 6. Intermediate visual effects and subsequent results of warm-start.

3) *Analyzing the effect of semantic loss:* We conducted experiments removing some classes, e.g., the car class (w/o Car), the person class (w/o Person), and the both (w/o Car&Person). We also conducted an experiment removing the semantic loss (w/o \mathcal{L}_{sem}). As shown in Fig. 7, the semantic loss makes the pedestrians and the cars stand out from the background as shown in (c). The impact of person class is more significant than the car class. This is because in the MFNet, pedestrians has a larger number than car. It is worth to finding that (b) is totally the same as (d), implying that the infrared information of other classes than pedestrian and car classes contribute less to the segmentation task.

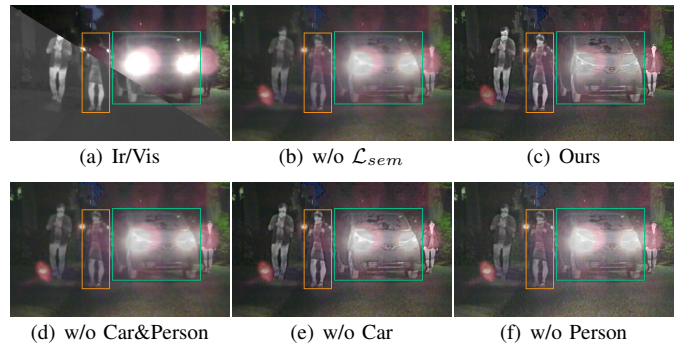


Fig. 7. Visual comparison by removing different semantic classes.

IV. CONCLUSION

In this letter, to break free from manually designing fusion rules, we develop a semantic-level fusion network with an adaptive semantic-driven training strategy to take full advantage of the guidance from the follow-up semantic tasks. Experimental results reveal that semantic loss can not only replace the manual design of fusion rules but also provide a flexible and robust semantic-level fusion that satisfies both human vision and high-level vision tasks.

REFERENCES

- [1] T. T. Zin, H. Takahashi, T. Toriu, and H. Hama, "Fusion of infrared and visible images for robust person detection," *Image fusion*, pp. 239–264, 2011.
- [2] Q. Ha, K. Watanabe, T. Karasawa, Y. Ushiku, and T. Harada, "Mfnet: Towards real-time semantic segmentation for autonomous vehicles with multi-spectral scenes," in *2017 IEEE/RSJ International Conference on Intelligent Robots and Systems (IROS)*, 2017, pp. 5108–5115.
- [3] J. Liu, X. Fan, Z. Huang, G. Wu, R. Liu, W. Zhong, and Z. Luo, "Target-aware dual adversarial learning and a multi-scenario multi-modality benchmark to fuse infrared and visible for object detection," in *Proceedings of the IEEE/CVF Conference on Computer Vision and Pattern Recognition (CVPR)*, June 2022, pp. 5802–5811.
- [4] L. Tang, J. Yuan, and J. Ma, "Image fusion in the loop of high-level vision tasks: A semantic-aware real-time infrared and visible image fusion network," *Information Fusion*, vol. 82, pp. 28–42, 2022.
- [5] Y. Sun, B. Cao, P. Zhu, and Q. Hu, "Defusion: A detection-driven infrared and visible image fusion network." New York, NY, USA: Association for Computing Machinery, 2022, p. 4003–4011.
- [6] Y. Liu, X. Chen, R. K. Ward, and J. Wang, "Image fusion with convolutional sparse representation," *IEEE Signal Processing Letters*, vol. 23, no. 12, p. 1882 – 1886, 2016.
- [7] X. Zhang, Y. Ma, F. Fan, Y. Zhang, and J. Huang, "Infrared and visible image fusion via saliency analysis and local edge-preserving multi-scale decomposition," *JOSA A*, vol. 34, no. 8, pp. 1400–1410, 2017.
- [8] J. Ma, C. Chen, C. Li, and J. Huang, "Infrared and visible image fusion via gradient transfer and total variation minimization," *Information Fusion*, vol. 31, pp. 100–109, 2016.
- [9] K. Hara, K. Inoue, and K. Urahama, "A differentiable approximation approach to contrast-aware image fusion," *IEEE Signal Processing Letters*, vol. 21, no. 6, pp. 742–745, 2014.
- [10] D. P. Bavirisetti, G. Xiao, and G. Liu, "Multi-sensor image fusion based on fourth order partial differential equations," in *2017 20th International conference on information fusion (Fusion)*. IEEE, 2017, pp. 1–9.
- [11] Y. Liu, X. Chen, R. K. Ward, and Z. J. Wang, "Medical image fusion via convolutional sparsity based morphological component analysis," *IEEE Signal Processing Letters*, vol. 26, no. 3, pp. 485–489, 2019.
- [12] R. Gao, S. A. Vorobyov, and H. Zhao, "Image fusion with cosparsity analysis operator," *IEEE Signal Processing Letters*, vol. 24, no. 7, pp. 943–947, 2017.
- [13] Y. Yang, W. Cao, S. Wu, and Z. Li, "Multi-scale fusion of two large-exposure-ratio images," *IEEE Signal Processing Letters*, vol. 25, no. 12, pp. 1885–1889, 2018.
- [14] Z. Jiang, Z. Zhang, X. Fan, and R. Liu, "Towards all weather and unobstructed multi-spectral image stitching: Algorithm and benchmark," in *Proceedings of the 30th ACM International Conference on Multimedia*, 2022, pp. 3783–3791.
- [15] K. Nomura, D. Sugimura, and T. Hamamoto, "Underwater image color correction using exposure-bracketing imaging," *IEEE Signal Processing Letters*, vol. 25, no. 6, pp. 893–897, 2018.
- [16] L. Ma, T. Ma, R. Liu, X. Fan, and Z. Luo, "Toward fast, flexible, and robust low-light image enhancement," in *Proceedings of the IEEE/CVF Conference on Computer Vision and Pattern Recognition (CVPR)*, June 2022, pp. 5637–5646.
- [17] H. Li and X.-J. Wu, "Densefuse: A fusion approach to infrared and visible images," *IEEE Transactions on Image Processing*, vol. 28, no. 5, pp. 2614–2623, 2019.
- [18] H. Li, X.-J. Wu, and J. Kittler, "Rfn-nest: An end-to-end residual fusion network for infrared and visible images," *Information Fusion*, vol. 73, pp. 72–86, 2021.
- [19] J. Liu, Y. Wu, Z. Huang, R. Liu, and X. Fan, "Smoa: Searching a modality-oriented architecture for infrared and visible image fusion," *IEEE Signal Processing Letters*, vol. 28, pp. 1818–1822, 2021.
- [20] V. Vs, J. M. J. Valanarasu, P. Oza, and V. M. Patel, "Image fusion transformer," in *2022 IEEE International Conference on Image Processing (ICIP)*. IEEE, 2022, pp. 3566–3570.
- [21] H. Xu, J. Ma, J. Jiang, X. Guo, and H. Ling, "U2fusion: A unified unsupervised image fusion network," *IEEE Transactions on Pattern Analysis and Machine Intelligence*, vol. 44, no. 1, pp. 502–518, 2022.
- [22] J. Ma, L. Tang, M. Xu, H. Zhang, and G. Xiao, "Stdffusionnet: An infrared and visible image fusion network based on salient target detection," *IEEE Transactions on Instrumentation and Measurement*, vol. 70, pp. 1–13, 2021.
- [23] J. Ma, L. Tang, F. Fan, J. Huang, X. Mei, and Y. Ma, "Swinfusion: Cross-domain long-range learning for general image fusion via swin transformer," *IEEE/CAA Journal of Automatica Sinica*, vol. 9, no. 7, pp. 1200–1217, 2022.
- [24] J. Ma, W. Yu, P. Liang, C. Li, and J. Jiang, "Fusiongan: A generative adversarial network for infrared and visible image fusion," *Information Fusion*, vol. 48, pp. 11–26, 2019.
- [25] Y. Liu, F. Mu, Y. Shi, and X. Chen, "Sf-net: A multi-task model for brain tumor segmentation in multimodal mri via image fusion," *IEEE Signal Processing Letters*, vol. 29, pp. 1799–1803, 2022.
- [26] J. Liu, X. Fan, J. Jiang, R. Liu, and Z. Luo, "Learning a deep multi-scale feature ensemble and an edge-attention guidance for image fusion," *IEEE Transactions on Circuits and Systems for Video Technology*, vol. 32, no. 1, pp. 105–119, 2022.
- [27] J. Liu, Y. Wu, G. Wu, R. Liu, and X. Fan, "Learn to search a lightweight architecture for target-aware infrared and visible image fusion," *IEEE Signal Processing Letters*, 2022.
- [28] D. Wang, J. Liu, X. Fan, and R. Liu, "Unsupervised misaligned infrared and visible image fusion via cross-modality image generation and registration," *arXiv preprint arXiv:2205.11876*, 2022.
- [29] H. Zhang, H. Xu, Y. Xiao, X. Guo, and J. Ma, "Rethinking the image fusion: A fast unified image fusion network based on proportional maintenance of gradient and intensity," in *Proceedings of the AAAI Conference on Artificial Intelligence*, vol. 34, no. 07, 2020, pp. 12 797–12 804.
- [30] J. Liu, J. Shang, R. Liu, and X. Fan, "Attention-guided global-local adversarial learning for detail-preserving multi-exposure image fusion," *IEEE Transactions on Circuits and Systems for Video Technology*, 2022.
- [31] J. Liu, X. Fan, J. Jiang, R. Liu, and Z. Luo, "Learning a deep multi-scale feature ensemble and an edge-attention guidance for image fusion," *IEEE Transactions on Circuits and Systems for Video Technology*, pp. 1–1, 2021.
- [32] Z. Shen, M. Zhang, H. Zhao, S. Yi, and H. Li, "Efficient attention: Attention with linear complexities," in *Proceedings of the IEEE/CVF Winter Conference on Applications of Computer Vision (WACV)*, January 2021, pp. 3531–3539.
- [33] A. Toet, "TNO Image Fusion Dataset," 4 2014. [Online]. Available: https://figshare.com/articles/dataset/TNO_Image_Fusion_Dataset/1008029
- [34] Y. Liu, S. Liu, and Z. Wang, "A general framework for image fusion based on multi-scale transform and sparse representation," *Information Fusion*, vol. 24, pp. 147–164, 2015.
- [35] J. Ma, H. Zhang, Z. Shao, P. Liang, and H. Xu, "Ganmcc: A generative adversarial network with multiclassification constraints for infrared and visible image fusion," *IEEE Transactions on Instrumentation and Measurement*, vol. 70, pp. 1–14, 2021.
- [36] A. M. Eskicioglu and P. S. Fisher, "Image quality measures and their performance," *IEEE Transactions on Communications*, vol. 43, no. 12, p. 2959 – 2965, 1995.
- [37] G. Cui, H. Feng, Z. Xu, Q. Li, and Y. Chen, "Detail preserved fusion of visible and infrared images using regional saliency extraction and multi-scale image decomposition," *Optics Communications*, vol. 341, pp. 199–209, 2015.
- [38] J. Hu, L. Shen, and G. Sun, "Squeeze-and-excitation networks," in *2018 IEEE/CVF Conference on Computer Vision and Pattern Recognition*, 2018, pp. 7132–7141.
- [39] L. Chen, H. Zhang, J. Xiao, L. Nie, J. Shao, W. Liu, and T.-S. Chua, "Sca-cnn: Spatial and channel-wise in convolutional networks for image captioning," in *2017 IEEE Conference on Computer Vision and Pattern Recognition (CVPR)*, 2017, pp. 6298–6306.